Journal of Molecular Structure 1035 (2013) 295–306

Contents lists available at SciVerse ScienceDirect

Journal of Molecular Structure

journal homepage: www.elsevier.com/locate/molstruc

Synthesis, multiple interactions and spectroscopy analysis of ethyl-4-[(benzoyl)-hydrazonomethyl]-3,5-dimethyl-1*H*-pyrrole-2-carboxylate: Through experimental and quantum chemical approaches

R.N. Singh *, Amit Kumar, R.K. Tiwari, Poonam Rawat

Department of Chemistry, University of Lucknow, University Road, Lucknow 226 007, India

HIGHLIGHTS

- FT-IR spectrum of the studied compound is recorded and compared with the theoretical results.
- The ^{1}H NMR spectrum has also been calculated using GIAO method.
- By using TD-DFT/6-31G method, electronic transitions for title compound are predicted.
- Dimer formation has been evaluated with the help of DFT and QTAIM theory.
- Chemical reactivity has been explained with the aid of global and local electronic descriptors.

ARTICLE INFO

Article history:
Received 17 June 2012
Received in revised form 31 October 2012
Accepted 31 October 2012
Available online 23 November 2012

Keywords:
Pyrrole hydrazide-hydrazone
Multiple interactions
Hydrogen bonded dimer
AIM calculation
Reactivity descriptors

ABSTRACT

The carboxaldehydes of pyrrole form important class of precursors for synthesis of acid hydrazide-hydrazones and their derivatives which show the various applications. A novel hydrazide-hydrazone of pyrrole: Ethyl-4-[(benzoyl)-hydrazonomethyl]-3,5-dimethyl-1*H*-pyrrole-2-carboxylate (**3**) has been synthesized by condensation of ethyl-4-formyl-3,5-dimetyl-1*H*-pyrrole-2-carboxylate and benzohydrazide. The product was characterized by spectroscopy methods (FT-IR, ^{1}H NMR, UV–Vis and DART Mass) and quantum chemical calculations. The calculated thermodynamic parameters show that the formation of (**3**) is exothermic and spontaneous at room temperature. The local electronic descriptors analysis and molecular electrostatic potential surface were used to predict the sites and nature of interactions which indicate the dimer formation through multiple interaction through N—H···O and C–H···O. The vibrational analysis shows red shifts in υ_{N-H} and $\upsilon_{C=O}$ as result of dimer formation. Topological and energetic parameters generated by AIM show the nature of interactions in dimer. The interaction energies of dimer formation using DFT and AIM calculations are found to be 14.19 and 15.19 kcal/mol respectively. Ellipticity analysis confirms the presence of resonance assisted heteronuclear H-bonding in dimer.

1. Introduction

The carboxaldehydes of pyrrole form important class of precursors for synthesis of hydrazones and their derivatives. Pyrrole fragment is a constituent of many biological systems. The pyrrole-α-carboxaldehyde has been used for the development of potential chemosensors [1]. Hydrazones are an important class of compounds due to their various properties and applications. They are used as antimicrobial, antitubercular [2–6] and antidiabetic agents [7]. They have strong coordinating ability towards different metal ions [8,9]. In addition, aroyl hydrazones and their mode of chelation with transition metal ions present in the living system have been of significant interest [10,11]. The chemical stability of hydrazones and their high melting point have recently made them attractive as prospective new material for opto-electronic applications [12]. Phenyl hydrazones exhibit a series of good organic nonlinear optical (NLO) properties [13,14]. Hydrazones having frame —CH=N—NH— constitute an important class of compounds for [2 + 2] cycloadditions, 1, 3 dipolar cycloadditions and have been turned into a valuable tool for the synthesis of azetidinones, pyrazoles, respectively [15,16] and various other N, O or S containing heterocyclic compounds such as oxadiazolines, thiazolidinones and triazolines [17–23].

Hydrogen bonds are of versatile importance in fields of chemistry and bio-chemistry governing molecular assemblies, supramolecular structures, chemical reactions and life processes. Intra- and intermolecular hydrogen bonds are classified in two

* Corresponding author. Tel.: +91 9451308205.
E-mail address: rnsvk.chemistry@gmail.com (R.N. Singh).

0022-2860/$ - see front matter © 2012 Elsevier B.V. All rights reserved.
http://dx.doi.org/10.1016/j.molstruc.2012.10.065

categories (i) classical or conventional hydrogen bonds and (ii) non-conventional or improper hydrogen bonds depending upon the nature of atoms or hydrogen bond donor and acceptor involved in the hydrogen bridges. Type of non-conventional hydrogen bonds are (i) those in which the nature of hydrogen bond donor is non-conventional as C—H group [24] (ii) the nature of hydrogen bond acceptor is non-conventional as C atom or π-system [25] (iii) both the donor and acceptor are non-conventional groups [26]. The title compound (**3**) was synthesized and characterized due to the various applications of hydrazones. In the present paper we report the molecular dimer structure of (**3**) through multiple interactions using quantum chemical calculations and experimental FT-IR spectrum. Quantum chemical calculations also provide further information on chemical reactivity of the title compound.

2. Experimental details

Benzohydrazide was prepared by refluxing the equimolar reaction mixture of ethylbenzoate and hydrazine hydrate in methanol. Ethyl-4-formyl-3,5-dimetyl-1*H*-pyrrole-2-carboxylate was prepared by an earlier reported method [27]. The ^{1}H NMR spectrum of (**3**) was recorded in DMSO-d_6 on Bruker DRX-300 spectrometer using TMS as an internal reference. The UV–Vis absorption spectrum of (**3**) (1×10^{-5} M in DMSO) was recorded on ELICO SL-164 spectrophotometer. The FT-IR spectrum was recorded in KBr medium on a Bruker spectrometer. The DART-Mass spectrum was recorded on JMS-T100LC, Accu TOF mass spectrometer.

2.1. Synthesis of ethyl-4-[(benzoyl)-hydrazonomethyl]-3,5-dimethyl-1H-pyrrole-2-carboxylate (*3*)

An ice cold solution of benzohydrazide (0.1394 g, 1.0251 mmol) in 20 ml methanol was added dropwise with stirring in 15 ml solution of Ethyl-4-formyl-3,5-dimetyl-1*H*-pyrrole-2-carboxylate (0.200 g, 1.0251 mmol) in methanol. Now, the reaction mixture was stirred for 32 h at room temperature, the precipitate of red color was appeared. The precipitate was filtered off, washed with methanol and dried in air. Yield: 41.83%. Compound decomposes above 250 °C without melting. ^{1}H NMR DMSO-d_6, δ (ppm): 1.278–1.323 (t, 3H, J = 6.75, CH3 ester); 2.369 (s, 3H, pyrrole-CH_3); 2.409 (s, 3H, pyrrole-CH3); 4.208–4.275 (q, 2H, J = 6.70, CH_2 ester); 7.859–7.889 (m, 3H, Ar—H); 8.363–8.396 (d, 2H, J = 9.90, Ar—H); 8.884 (s, 1H, CH=N); 11.049 (s, 1H, hydrazide-NH); 11.623 (s, 1H, pyrrole-NH). UV–Vis absorption spectrum (1×10^{-5} M in DMSO): λ_{max} (nm): 226 nm, 308 nm. DART Mass: Observed m/z 314.1953 [M^++1], Calc. 313.1426 amu.

3. Computational methods

The theoretical calculations for the synthesized compound were carried out with Gaussian 03 program package [28] to predict the molecular structure, ^{1}H NMR chemical shifts and vibrational wavenumbers using density functional theory (DFT), B3LYP functional and 6-31G(d,p) basis set. B3LYP invokes Becke's three parameter (local, non local, Hartree–Fock) hybrid exchange functional (B3) [29] with Lee–Yang–Parr correlation functional (LYP) [30]. The basis set 6-31G(d,p) with 'd' polarization functions on heavy atoms and 'p' polarization functions on hydrogen atoms are used for better description of polar bonds [31,32]. It should be emphasized that 'p' polarization functions on hydrogen atoms are used for reproducing the out of plane vibrations involving hydrogen atoms. Convergence criterion in which both the maximum force and displacement are smaller than the cutoff values of 0.000450 and 0.001800 and r.m.s. force and displacement are less than the cutoff values of 0.000300 and 0.001200 are used in the calculations. The absence of imaginary frequency verified that stationary points correspond to minima of the potential energy surfaces. The time dependent density functional (TD-DFT) is carried out to find the electronic transitions. The optimized geometrical parameters are used in the calculation of vibrational wavenumbers to characterize all stationary points as minima and their harmonic vibrational wavenumbers are positive. All molecular structures are visualized using software Chemcraft [33] and Gauss-View [34]. Potential energy distribution along internal coordinates is calculated by Gar2ped software [35]. Internal coordinate system recommended by Pulay et al. is used for the assignment of vibrational modes [36]. To estimate the enthalpy and Gibbs free energy values, thermal corrections to enthalpy and Gibbs free energy calculated at B3LYP/6-31G(d,p) level were added to the calculated total energies. The wave function file generated at B3LYP/6-31G(d,p) basis set from the optimized coordinate was used to calculate the topological parameters by AIM 2000 1.0 software [37]. Bader's theory of atoms in molecules (AIM) theory efficiently describes the nature and strength of various types of hydrogen-bonded interactions. One of the advantages of the AIM theory is its ability to provide information on changes in the electron density distribution as result of either bond formation or complex formation. The basis set reliability and stability in the values of AIM parameters have been studied and found that they are almost independent of basis set in case of used functional B3LYP in both DFT and AIM calculations [38].

4. Results and discussion

4.1. Thermodynamic properties

For simplicity, reactants ethyl-4-formyl-3,5-dimetyl-1*H*-pyrrole-2-carboxylate, benzohydrazide, product ethyl-4-[(benzoyl)-hydrazonomethyl]-3,5-dimethyl-1*H*-pyrrole-2-carboxylate and water as a byproduct are abbreviated as **1**, **2**, **3** and **4** respectively. Calculated Enthalpy (H), Gibbs free energy (G) and Entropy (S) of reactants (**1**, **2**) and products (**3**, **4**) at room temperature is listed in Table 1. For reaction, enthalpy change ($\Delta H_{Reaction}$), Gibbs free energy change ($\Delta G_{Reaction}$) and entropy change ($\Delta S_{Reaction}$) are calculated from thermodynamic parameters of reactants and products at room temperature and found to be −3.41, −1.63 kcal/mol and −5.94 cal mol^{-1} K^{-1} respectively. The negative values for $\Delta H_{Reaction}$ and $\Delta G_{Reaction}$ show that the reaction is exothermic and spontaneous at room temperature. Thermodynamic relation between equilibrium constant (K_{eq}) and Gibbs free energy change of reaction ($\Delta G_{Reaction}$) at temperature (T) is given as $K_{eq} = e^{-\Delta G/RT}$. The value of equilibrium constant (K_{eq}) determines the nature of reaction: (i) if $K_{eq} > 1$, reaction is favored in forward direction, (ii) if $K_{eq} = 0$, reaction is in equilibrium state, and (iii) if $K_{eq} < 1$, reaction is favored in backward direction at temperature (T). Using above equation, equilibrium constant (K_{eq}) for title reaction is calculated as 60.27 at room temperature. Therefore, reaction is favored in forward direction at room temperature. This confirms the formation of product (**3**) at room temperature.

The binding energy of dimer is calculated as 14.19 kcal/mol using DFT calculation. The calculated hydrogen binding energy of

Table 1
Calculated Enthalpy (H), Gibbs free energy (G) and Entropy (S) of reactants (**1**,**2**) and products (**3**,**4**) at room temperature, using B3LYP/6-31G(d,p) at (25 °C).

Thermodynamic parameters	1	2	3	4
H (a.u.)	−669.12	−456.12	−1048.85	−76.39
G (a.u.)	−669.18	−456.16	−1048.93	−76.41
S (kcal mol^{-1} K^{-1})	124.94	92.98	166.86	45.11

Table 2
Calculated Enthalpy (H), Gibbs free energy (G), Entropy (S), their change and equilibrium constant (K_{eq}) of conversion from monomer to dimer at (25 °C).

Parameters	Enthalpy (H) a.u.	Gibbs free energy (G) a.u.	Entropy (S) (cal mol^{-1} K^{-1})	ΔH (kcal/mol)	ΔG (kcal/mol)	ΔS (cal mol^{-1} K^{-1})	K_{eq}
2 × Monomer	−2097.71	−2097.87	333.73	−12.70	−2.42	−34.45	60.27
Dimer	−2097.73	−2097.87	299.28				

dimer formation has been corrected for the basis set superposition error (BSSE) via the standard counterpoise method [39] and found to be 10.63 kcal/mol. The changes in thermodynamic parameters during the dimer formation in gaseous phase have the negative values of ΔH (kcal/mol), ΔG (kcal/mol) and ΔS (cal mol^{-1} K^{-1}) and incorporated in Table 2, indicating that the dimer formation is exothermic and spontaneous. The high value of equilibrium constant (K_{eq} = 60.27) between monomer and dimer indicates that dimer formation is more preferred and as result even *anti* conformer gets converted to *syn* and finally changes into dimer.

4.2. Molecular geometry

Geometry of all the reactants and products involved in chemical reaction was computed at B3LYP/6-31G(d,p) level. The product molecule (**3**) has many stable conformers but global minimum and another having next low-lying minimum conformers have been incorporated in considering the dimer formation and comparing with experimental spectral values in the discussion. The reported optimized ground state *syn* and *anti* stable conformers are as the global minimum and the next low-lying minimum on the potential energy surface. Molecular geometry was drawn considering both obtained spectral data of this synthesized compound (**3**) and the structural pattern reported in single crystal structure of the other hydrazide-hydrazone obtained from the reaction of acid hydrazides with aromatic aldehydes [40]. The conformers were determined from drawn geometry by systematic search using potential energy surface scan around different dihedral angle, but the global minima and another next low-lying minimum resulted around the dihedral angle τ $C_3C_2C_9O_{20}$. The idea from reported literature on singe crystals, determining method and the calculated energy values for conformers of product (**3**) provided the basis for principle involved in discussion. Optimized geometry of the ground state *syn* and *anti* conformer is shown in Fig. 1, with atom numbering. They have energy −1049.2206 and −1049.2202 a.u. respectively at room temperature. They have energy difference 0.2397 kcal/mol and exist in ratio 59.42%, 40.48% respectively at room temperature. The asymmetry in the N1—C2 and N1—C5 bonds arises due to the presence of opposite nature groups such as ethoxycarbonyl (electron withdrawing) group at C2 and methyl (electron donating) group at C5 of pyrrole ring. It leads to the elongation of N1—C2 bond. These effects are not only observed in quantum calculation but also reflect in crystal structure of the ethyl-3,5-dimethyl-1*H*-pyrrole-2-carboxylate [41], methyl 4-p-tolyl-1*H*-pyrrole-2-carboxylate [42] and other pyrrole-2-carboxylate derivatives [43]. Optimized geometry of dimer is shown in

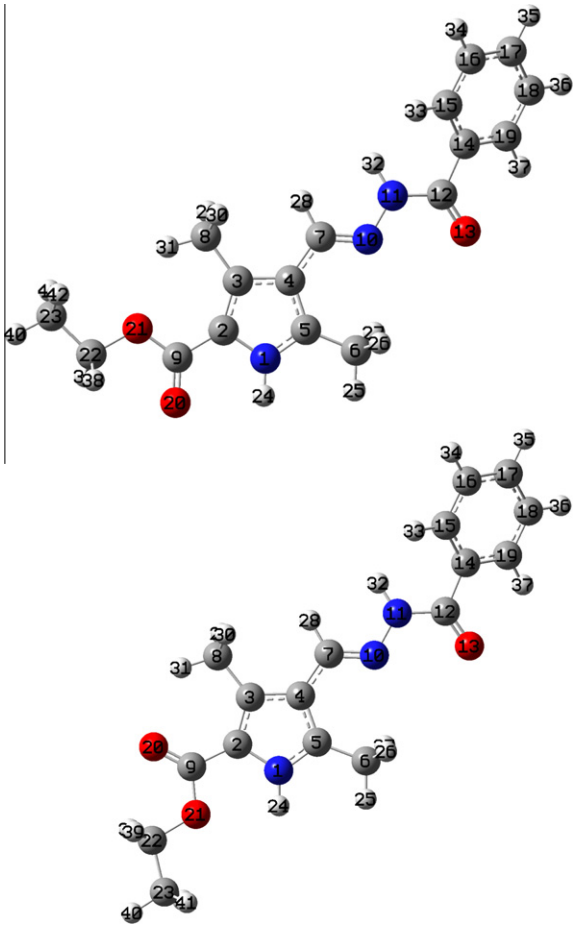

Fig. 1. Optimized geometry of *syn* and *anti* conformer of (**3**) using B3LYP/6-31G(d,p).

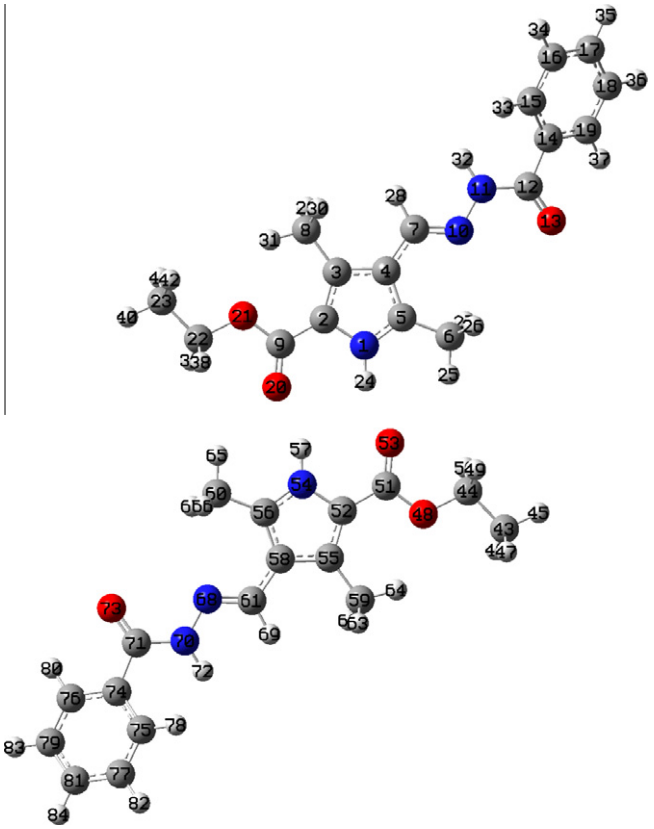

Fig. 2. Optimized geometry of dimer for *syn*-conformer using B3LYP/6-31G(d,p).

Table 3
Selected optimized geometrical parameters from molecular dimer of (**3**) calculated at B3LYP/6-31G(d, p): bond length (Å), bond angle (°) and dihedral angle (°).

Bond length	(Å)	Bond angle	(°)	Dihedral angle	(°)
R(1,2)	1.3888	A(2,1,5)	110.7402	D(5,1,2,3)	−0.0133
R(1,5)	1.3474	A(2,1,24)	124.8666	D(2,1,5,4)	0.0046
R(1,24)	1.0203	A(5,1,24)	124.3931	D(1,2,3,4)	0.0161
R(2,3)	1.3983	A(1,2,3)	107.6694	D(1,2,9,21)	−179.882
R(2,9)	1.4485	A(1,2,9)	117.9231	D(2,3,4,5)	−0.0135
R(3,4)	1.4251	A(3,2,9)	134.4074	D(2,3,8,29)	−119.213
R(3,8)	1.5010	A(2,3,4)	106.3910	D(3,4,5,1)	0.0056
R(4,5)	1.4103	A(2,3,8)	128.3132	D(3,4,7,10)	−179.970
R(4,7)	1.4456	A(4,3,8)	125.2957	D(1,5,6,25)	2.3165
R(5,6)	1.4916	A(3,4,5)	107.8297	D(4,7,10,11)	−179.686
R(6,25)	1.0920	A(3,4,7)	125.5677	D(28,7,10,11)	0.4789
R(7,10)	1.2891	A(5,4,7)	126.6019	D(2,9,20,57)	−0.1615
R(7,28)	1.0998	A(1,5,4)	107.3698	D(21,9,20,57)	179.8210
R(8,29)	1.0968	A(1,5,6)	122.3102	D(2,9,21,22)	179.9848
R(9,20)	1.2320	A(4,5,6)	130.3199	D(20,9,21,22)	0.0006
R(9,21)	1.3503	A(5,6,25)	110.3442	D(7,10,11,12)	−172.757
R(10,11)	1.3638	A(4,7,10)	122.4269	D(7,10,11,32)	−3.8726
R(11,12)	1.3839	A(4,7,28)	116.6984	(10,11,12,13)	1.4964
R(11,32)	1.0168	A(10,7,28)	120.8746	(10,11,12,14)	−179.252
R(12,13)	1.2206	A(2,9,20)	124.0002	(32,11,12,13)	−167.387
R(12,14)	1.5039	A(2,9,21)	114.1186	(32,11,12,14)	11.8646
R(14,15)	1.4025	A(20,9,21)	121.8812	(11,12,14,15)	27.0989
R(14,19)	1.4014	A(7,10,11)	116.5603	(11,12,14,19)	−154.645
R(15,16)	1.3951	A(10,11,12)	120.6972	(13,12,14,15)	−153.642
R(15,33)	1.0863	A(10,11,32)	119.1853	(13,12,14,19)	24.6149
R(16,17)	1.3955	A(12,11,32)	119.1889	(12,14,15,16)	179.3526
R(16,34)	1.0860	A(11,12,13)	123.3290	(12,14,19,18)	−179.85
R(17,18)	1.3973	A(11,12,14)	114.2605	(14,15,16,17)	−0.0259
R(17,35)	1.0861	A(13,12,14)	122.4061	(15,16,17,18)	−0.7158
R(18,19)	1.3922	A(12,14,15)	123.7543	(16,17,18,19)	0.3393
R(22,23)	1.5164	A(15,16,17)	120.0825	(17,18,19,14)	0.7827
R(22,38)	1.0943	A(16,17,18)	119.8538	D(9,21,22,23)	179.8415
R(23,40)	1.0942	A(17,18,19)	120.1151	(21,22,23,41)	60.3452
R(24,53)	1.9074	A(17,18,36)	120.0421	D(2,1,24,53)	179.1416
R(20,57)	1.9073	A(14,19,18)	120.4187	D(9,20,57,54)	−179.439
R(25,53)	2.59585	A(9,21,22)	116.3813	D(6,25,53,51)	−177.351
R(20,65)	2.59574	A(21,22,23)	107.4846	D(60,65,20,9)	−177.339
R(1,53)	2.88753	A(1,24,53)	160.0303		
R(54,20)	2.88741	A(54,57,20)	160.0251		
R(6,53)	3.5009	A(6,25,53)	139.7314		
R(60,20)	3.5008	A(60,65,20)	139.7288		

Table 4
Experimental and calculated GIAO ^{1}H NMR chemical shifts of (**3**) using B3LYP/6-31G(d,p) in DMSO-d_6 as the solvent δ_{Exp}.

Atom no.	δ_{Cal}	δ_{Exp}	Assignment
H24	9.182	11.623	(s, 1H, pyrrole-NH)
H25	2.148	2.409	(s, 3H, pyrrole α-CH3)
H26	2.638		
H27	2.589		
H28	7.950	8.884	(s, 1H, proton of CH═N)
H29	2.304	2.369	(s, 3H, pyrrole β-CH_3)
H30	2.139		
H31	2.366		
H32	8.204	11.049	(s, 1H, hydrazide-NH)
H33	7.978	8.363–8.396	(d, 1H, *o*-H of benzene ring with *J* = 9.90 Hz)
H34	7.810	7.859–7.889	(m, 3H, *m*- and *p*-protons of benzene ring)
H35	7.917		
H36	7.849		
H37	8.273	8.363–8.396	(d, 1H, *o-H* of benzene ring with *J* = 9.90, Ar—H)
H38	4.299	4.208–4.275	(q, 2H, *J* = 6.70, CH_2 ester)
H39	4.320		
H40	1.209	1.278–1.323	(t, 3H, *J* = 6.75, CH3 ester)
H41	1.472		
H42	1.485		

Abbreviations: s = singlet, t = triplet, q = quartet, d = doublet, m and p meta and para position hydrogen atom in benzene ring.

Fig. 2, with atom numbering. Selected optimized geometrical parameters of dimer of (**3**) are listed in Table 3. In dimer, heteronuclear intermolecular hydrogen bonding (N—H···O) between pyrrolic (N—H) and carbonyl (C═O) oxygen of ester form two hydrogen bonds. In intermolecular hydrogen bonds, the N—H bond acts as proton donor and C═O bond as proton acceptor. According to the Etter terminology [44], the cyclic ester dimer form the ten member pseudo ring denoted as $R_2^2(10)$ or more extended sixteen member pseudo ring $R_2^2(16)$. The superscript designates the number of acceptor centers and the subscript, the number of donors in the motif. In dimer, due to intermolecular hydrogen-bond formation both proton donor (N—H bond) and proton acceptor (C═O bond) are elongated from 1.0105 Å to 1.0203 Å, 1.2238 Å to 1.2320 Å respectively. Total energy of the monomer (*syn*-conformer) and its dimer are calculated as −1049.22060088, −2098.46381691 a.u. respectively.

4.3. ^{1}H NMR spectroscopy

Isotropic magnetic shielding of optimized TMS and product are calculated with GIAO approach using B3LYP functional and 6-31G(d,p) basis set [45]. ^{1}H NMR Chemical shift of any proton is the difference between isotropic magnetic shielding of TMS and that proton. Experimental and calculated ^{1}H NMR chemical shifts of the title compound are listed in Table 4. The experimental ^{1}H NMR spectrum is given in Fig. 3. In order to compare the chemical shifts, correlation graph between the experimental and calculated

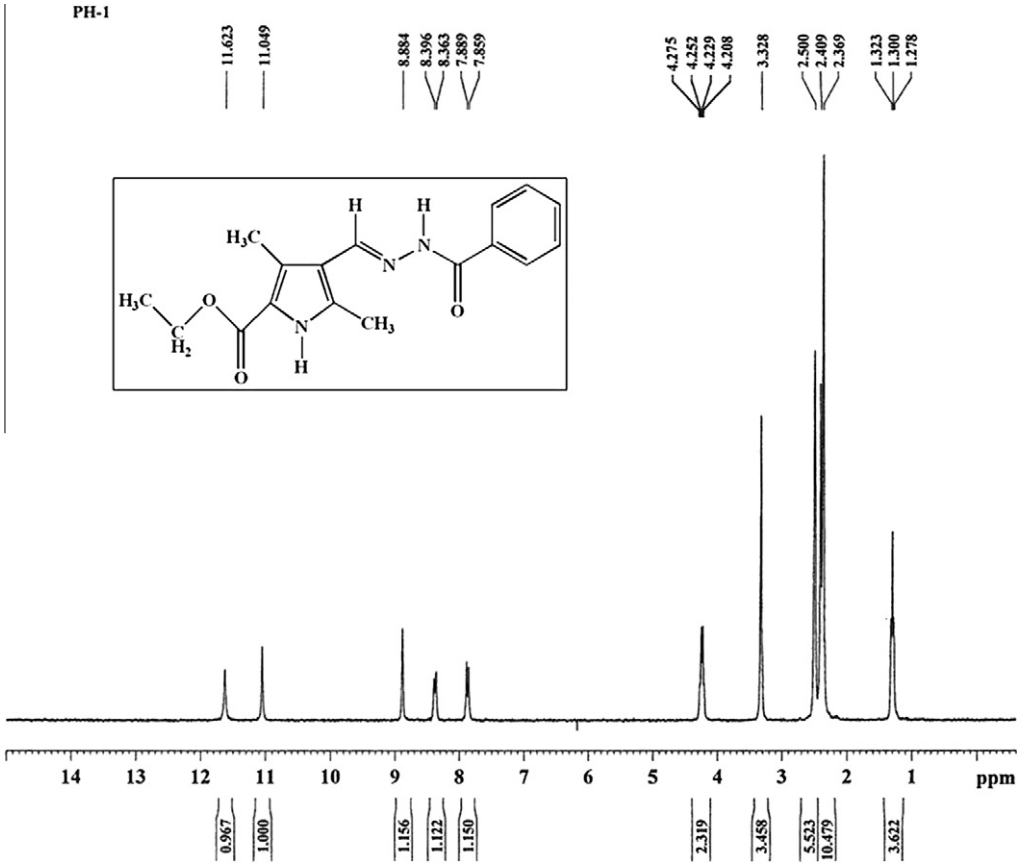

Fig. 3. The experimental ^{1}H NMR spectrum of the studied compound.

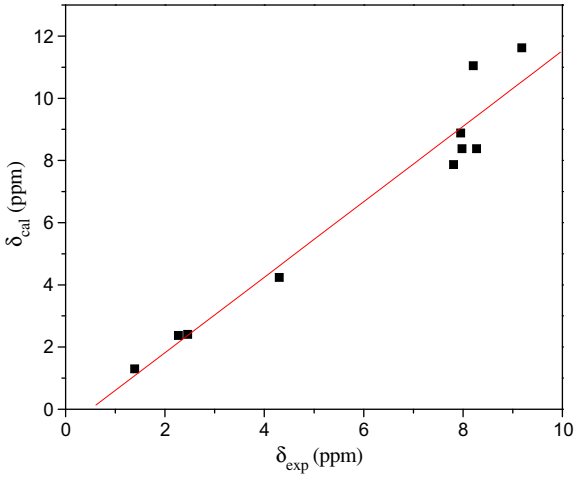

Fig. 4. Correlation graph between experimental and calculated ^{1}H NMR chemical shifts (δ) in (ppm).

chemical shifts is shown in Fig. 4. The correlation graph follow the linear equation ($y = 0.7799x - 0.7991$), where 'y' is the experimental ^{1}H NMR chemical shift, 'x' is the calculated ^{1}H NMR chemical shift. The high value of correlation coefficient ($R^2 = 0.94$) shows that there is a good agreement between experimental and calculated chemical shifts.

4.4. UV–Vis spectroscopy

The electronic transitions of the product were calculated using time dependent density functional (TD-DFT) theory. The nature of the transitions observed in the UV–Vis spectrum of (**3**) has been studied by the comparison between experimental and calculated electronic transitions and are listed in Table 5. The experimental and theoretical UV–Vis spectrum is shown in Fig. 5. The selected molecular orbital plots involved in electronic excitations for (**3**) are given in Fig. 6. The FMOs are important in determine the ability of a molecule to absorb light and molecular reactivity. The vicinal orbitals of HOMO and LUMO play the role of electron donor and electron acceptor respectively. From the charge transfer viewpoint, the high value of $|\varepsilon_{HOMO}|$ means that the ionization is more difficult, that is to say, that molecule is hard to lose electron. The HOMO–LUMO energy gap is an important stability index. The high value of HOMO–LUMO energy gap of title molecule reflects the chemical stability of the molecule.

HOMO energy = −5.4757 eV
LUMO energy = −1.2188 eV
HOMO—LUMO energy gap = 4.2569 eV

TD-DFT calculations using B3LYP/6-31G(d,p), predict three intense electronic transitions at $\lambda_{max} = 241.06$ nm, $f = 0.4149$; $\lambda_{max} = 272.30$ nm, $f = 0.2528$ and $\lambda_{max} = 327.23$ nm, $f = 0.8430$. The calculated electronic transitions at $\lambda_{max} = 241.06$ nm and $\lambda_{max} = 327.23$ nm are in agreement with the experimental electronic transitions observed at λ_{max} 226, 308 nm respectively. The calculated values for wavelength of maximum absorption (λ_{max}) are also in agreement with the reported λ_{max} in literature [46]. The experimental bands at 226 and 308 nm originate mainly due to the H-1→L + 1, H → L electronic excitation respectively.

According to the NBO analyses, H-1 → L + 1, H → L electronic excitations show π(C4—C5) → π^*(C7—N10) and n(O13) → π^* (C9—O20) transitions respectively. The results show that the

Table 5
Comparison between experimental and calculated electronic transitions: E (eV), oscillatory strength (f), λ_{max} (nm) using TD-DFT/B3LYP/6-31G(d,p) in DMSO at (25 °C).

S. no.	Electronic transitions	E (eV)	Calculated λ_{max} (nm)	Oscillator strength (f)	% Contribution	Assignment	Observed λ_{max} (nm)
1	H → L	3.78	327.23	0.8430	44.89	$\pi \rightarrow \pi^*$	308
2	H-4 → L	4.55	272.3	0.2528	2.19	$\pi \rightarrow \pi^*$	
	H-2 → L				1.45		
	H-1 → L				32.75		
	H → L + 1				9.99		
3	H-1 → L + 1	5.14	241.06	0.4149	39.62	$n \rightarrow \pi^*$	226
4	H-4 → L	5.44	227.57	0.0989	1.35	$\pi \rightarrow \pi^*$	
	H-2 → L				1.62		
	H-2 → L + 2				1.28		
	H-1 → L + 2				38.35		

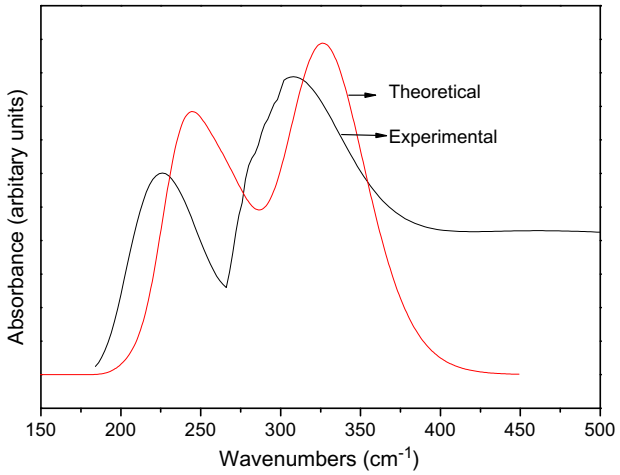

Fig. 5. Comparison between experimental and theoretical UV–Vis spectrum.

charge transfer (CT) occurs from the proton acceptor nonbonding n(O) orbital of carbonyl to the proton donor σ^*(N—H) orbital of pyrrole.

4.5. Vibrational spectroscopy

The experimental and theoretical (selected) vibrational wavenumbers of dimer at B3LYP/6-31G(d,p) level and their assignments using PED are given in Table 6. The calculated (monomer, dimer) and the experimental FT-IR spectra of (**3**) in the region 4000–400 cm^{-1} are shown graphically in Fig. 7. The total number of atoms in monomer and dimer are 42 and 84 which give 120 and 246, $(3n - 6)$ vibrational modes for monomer and dimer respectively. The calculated vibrational wavenumbers have higher values than their experimental for most of the normal modes. Two factors may be responsible for the discrepancies between the experimental and computed wavenumbers of this compound. The first is caused by difference of the environment (gas and solid phase) and the second is due to the fact that the experimental values are anharmonic wavenumbers while the calculated values are harmonic ones. Therefore, calculated wavenumbers at B3LYP/6-31G(d,p) level are scaled down using single scaling factor 0.9608 [47], to discard the anharmonicity present in real system. The correlation graph is shown in Fig. 8. The value of correlation coefficient found to be $r^2 = 0.99$. The observed wavenumbers are in good agreement with the calculated wavenumbers of dimer than monomer. Therefore, observed wavenumbers are assigned using dimer PED.

In the experimental FT-IR spectrum of (**3**), the N—H stretch of pyrrole (ν_{NH}) is observed at 3301 cm^{-1}, whereas it is calculated as 3341 cm^{-1} in dimer and 3502 cm^{-1} in monomer. The observed wavenumber at 3301 cm^{-1} is in good agreement with the calculated wavenumber of dimer. The observed value of ν_{NH} also correlates with the earlier reported strong absorption at 3358 cm^{-1} for hydrogen bonded pyrrole-2-carboxylic acid dimer recorded in KBr pellet, but it deviates to the reported free ν_{NH} band

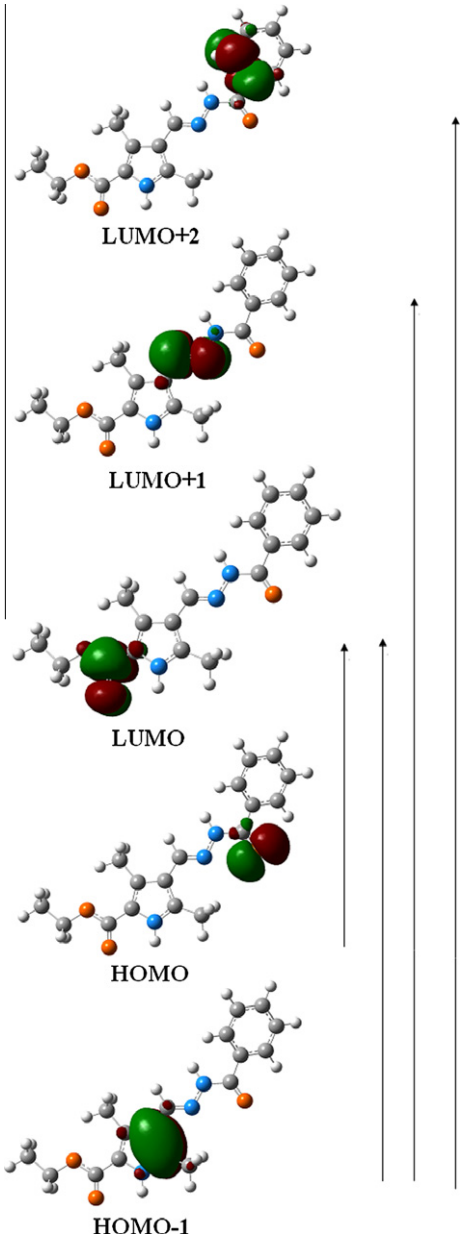

Fig. 6. Selected molecular orbital plots involved in electronic excitations for (**3**).

Table 6
Experimental and theoretical (selected) vibrational wavenumbers of dimer using B3LYP/6-31G(d,p) and their assignments [harmonic vibrational wavenumbers (cm^{-1}), IR_{int} ($Kmmol^{-1}$)].

Mode no.	Wavenumbers		Intensity	Exp. waven-umbers	Assignment [PED (>5%)]
	Unscaled	Scaled			
245	3511	3373	25.09	3391	ν(N11H32)(53) – ν(N70H72)(46)
244	3477	3341	2732.37	3301	ν(N1H24)(50) – ν(N54H57)(49)
241	3221	3095	11.84		ν(C76H80)(61) – ν(C19H37)(28) + ν(C79H83)(6)
239	3207	3081	46.74	3110	ν(C17H35)(21) – ν(C81H84)(21) + ν(C16H34)(17) – ν(C77H82)(17) + ν(C18H36)(6) – ν(C79H83)(6)
238	3196	3071	40.65		ν(C18H36)(20) – ν(C79H83)(19) – ν(C16H34)(17) + ν(C77H82)(16) – ν(C15H33)(8) + ν(C75H78)(8)
231	3178	3054	14.26		ν(C15H33)(27) – ν(C16H34)(20) – ν(C75H78)(18) + ν(C77H82)(13) + ν(C17H35)(10) – ν(C81H84)(6)
228	3139	3016	65.18	2976	ν(C23H41)(19) – ν(C23H42)(19) + ν(C43H46)(16) – ν(C43H47)(16) – (τ – C43C44)(7)
226	3132	3009	47.24		ν(C23H40)(34) – ν(C43H45)(31) – ν(C23H42)(9) – ν(C23H41)(9) + ν(C43H47)(8) + ν(C43H46)(8)
222	3106	2984	12.72		ν(C22H38)(26) – ν(C22H39)(25) + ν(C44H49)(13) – ν(C44H50)(13) + ν(C23H41)(5) – ν(C23H42)(5)
220	3081	2961	30.01		ν(C8H30)(45) – ν(C8H29)(42) + ν(C59H63)(6) – ν(C59H62)(6)
218	3064	2944	52.33	2928	ν(C22H39)(25) + ν(C22H38)(25) – ν(C44H50)(24) – ν(C44H49)(23)
215	3057	2937	18.34		ν(C6H26)(13) – (τ-H25O53)(13) – ν(C60H66)(12) + ν(C6H25)(10) + ν(C6H27)(9) – ν(C60H67)(9) – ν(C60H65)(9) – (δas-Me1)(8) + (τ-H65O20)(6)
213	3056	2936	29.91		ν(C43H45)(20) + ν(C43H47)(19) + ν(C43H46)(19) – ν(C23H40)(14) – ν(C23H42)(13) – ν(C23H41)(13)
211	3037	2918	111.05		ν(C59H62)(24) – ν(C8H29)(23) + ν(C59H63)(22) – ν(C8H30)(21)
209	3023	2904	90.66	2863	ν(C61H69)(49) – ν(C7H28)(45)
208	1782	1712	503.02		ν(C71O73)(27) – (δas-Me1)(15) + (τ-C5C6)(5) + (δas-Me1)(5)
206	1724	1656	2001.56	1669	ν(C51O53)(26) – ν(C9O20)(26) – (δas-Me1)(8) + (τ-C5C6)(6)
203	1685	1619	311.13	1619	(τ-C5C6)(31) – (δas-Me1)(28) – (τ-C60C56)(10) + (δas-Me1)(9) – ν(C61N68)(6) + ν(C7N10)(6)
199	1636	1571	9.44		ν(C79C81)(11) – ν(C77C81)(10) + ν(C74C75)(8) – ν(C17C18)(8) + ν(C16C17)(8)-ν(C74C76)(7) – ν(C14C15)(7) + ν(C14C19)(6) – (δas-R1)(5)
197	1607	1544	454.78		(τ-C5C6)(27) – (ρ-Me1)(27) + (δas-Me1)(9) – (τ-C60C56)(9) + (ρ-Me1)(8)
195	1569	1508	934.33	1500	(δas-Me1)(56) – (δas-Me1)(18) – (τ-C5C6)(11) – (ρ-Me1)(7)
194	1562	1501	243.1		(δas-Me1)(49) – (τ-C5C6)(24) – (δas-Me1)(15) + (τ-C60C56)(8)
189	1532	1472	57.69		(δas-Me1)(45) – (τ-C5C6)(25) – (δas-Me1)(14) + (τ-C60C56)(8)
188	1524	1464	52.27		(δas-Me1)(53) – (τ-C5C6)(19) – (δas-Me1)(17) + (τ-C60C56)(6)
182	1500	1441	11.99		(τ-C43C44)(34) + (δas-Me1)(14) + (δas-Me1)(8)
180	1498	1439	77.93		(δas-Me1)(49) – (τ-C5C6)(26) – (δas-Me1)(15) + (τ-C60C56)(8)
177	1491	1433	101.07	1433	(δas-Me1)(43) – (τ-C5C6)(33) – (δas-Me1)(13) + (τ-C60C56)(10)
173	1486	1428	41.91		(δas-Me1)(49) – (τ-C5C6)(25) – (δas-Me1)(15) + (τ-C60C56)(8)
171	1467	1409	405.4	1417	(δas-Me1)(38) – (τ-C5C6)(37) – (δas-Me1)(12) + (τ-C60C56)(12)
168	1429	1372	96.19		(τ-C5C6)(28) + (τ-H25O53)(21) – (δas-Me1)(15) – (τ-H65O20)(11) – (τ-C60C56)(9) + (δs-Me1)(6) + (δas-Me1)(5)
165	1426	1370	30.83		(τ-C5C6)(40) – (δas-Me1)(34) – (τ-C60C56)(14) + (δas-Me1)(12)
164	1415	1360	72.15	1364	(τ-C5C6)(42) – (δas-Me1)(34) – (τ-C60C56)(13) + (δas-Me1)(11)
161	1395	1340	44.63		(τ-C5C6)(41) – (δas-Me1)(35) – (τ-C60C56)(13) + (δas-Me1)(11)
157	1358	1304	42.81		(τ-C5C6)(44) – (δas-Me1)(30) – (τ-C60C56)(14) + (δas-Me1)(10)
153	1320	1268	1015.84	1254	(τ-C5C6)(46) – (δas-Me1)(28) – (τ-C60C56)(15) + (δas-Me1)(9)
149	1269	1219	423.98	1211	(τ-C5C6)(51) – (τ-C60C56)(16) – (δas-Me1)(14) – (ρ-Me1)(8)
148	1260	1211	526.05		(τ-C5C6)(52) – (τ-C60C56)(17) – (δas-Me1)(14) – (ρ-Me1)(9)
145	1223	1175	579.43	1134	(τ-C5C6)(45) – (ρ-Me1)(17) – (τ-C60C56)(14) + (ρ-Me1)(5)
143	1206	1159	110.12		(τ-C5C6)(26) – (τ-C60C56)(8) – (ω-C81H84)(7) + δ(C15H34C16)(6) – (ρ-Me1)(6) – (δas-Me1)(5) + δ(C74H78C75)(5) + δ(C16H33C15)(5)
137	1171	1125	441.2	1101	(τ-C5C6)(51) – (τ-C60C56)(16) – (ρ-Me1)(16) – (δas-Me1)(6) + (ρ-Me1)(5)
135	1142	1098	45.63		(τ-C5C6)(18) + (ρ-Me)(11) – (ρ-Me)(10) – (τ-C60C56)(6) + (δsc-C44C43O48)(6)-ν(C43C44)(6) + ν(C22C23)(5)
134	1130	1086	284.77	1058	(τ-C5C6)(50) – (τ-C60C56)(16) – (δas-Me1)(15) – (ρ-Me1)(7) + (δas-Me1)(5)
129	1095	1052	43.55	1032	(τ-C5C6)(54) – (τ-C60C56)(17) – (ρ-Me1)(11) – (δas-Me1)(10)
124	1058	1016	22.2		(τ-C5C6)(42) – (ρ-Me1)(16) – (τ-C60C56)(13) – (δas-Me1)(8) + (τ-H25O53)(5) + (ρ-Me1)(5)
121	1051	1010	66.97	973	(τ-C5C6)(51) – (τ-C60C56)(16) – (ρ-Me1)(12) – (δas-Me1)(11)
120	1047	1006	15.95		(τ-C5C6)(53) – (τ-C60C56)(17) – (δas-Me1)(11) – (ρ-Me1)(10)
105	931	895	56.4	879	(τ-C5C6)(51) – (ρ-Me1)(16) – (τ-C60C56)(16) + (ρ-Me1)(5)
103	903	868	8.65		(τ-C5C6)(50) – (τ-C60C56)(16) – (ρ-Me1)(12) – (δas-Me1)(8)
101	867	833	13.37	844	(τ-C5C6)(28) – (τ-C60C56)(9) – (ρ-Me1)(8) – (δ-O53O48C51)(6)
97	824	791	83.92	831	(τ-C5C6)(51) – (τ-C60C56)(16) – (ρ-Me1)(15) – (δas-Me1)(7) + (ρ-Me1)(5)
96	822	790	115.46	774	(ω-N54H57)(34) – (τ-H57O20)(31) + (ω-N1H24)(14) – (τ-H24O53)(13)
90	763	733	11.67		(δas-Me1)(16) – (ω-N54H57)(8) + (τ-H57O20)(7) – (δas-Me1)(5)
88	747	718	12.8		(ω-C51C52)(30) + (ω-C2C9)(30) – (ω-C51C52)(16) – (ω-C2C9)(13)

(*continued on next page*)

Table 6 (*continued*)

Mode no.	Wavenumbers		Intensity	Exp. waven-umbers	Assignment [PED (>5%)]
	Unscaled	Scaled			
86	720	692	66.9	695	(τ-C5C6)(34) – (τ-R)(15) + (τ-C60C56)(10) – (τ-R)(10) – (ω-C5C6)(9)
80	694	667	84.47	655	(τ-C5C6)(44) – (τ-C60C56)(14) – (τ-R)(10) + (τ-R)(7) – (ω-C5C6)(6)
76	637	612	11.17		(ω-C51C52)(19) + (ω-C2C9)(15) + (τ-C51C52)(14) + (τ-C2C9)(11) – (τ-R)(7) + (ω-C51C52)(5) + (ω-C2C9)(5)
70	533	512	31.49	511	(ρ-Me1)(19) – (τ-C5C6)(18) + (δas-Me1)(8) – (ω-C5C6)(6) + (ρ-Me1)(6) – (ω-C51C52)(6) – (τ-C60C56)(6) – (ω-C2C9)(5)
66	457	440	19.97	439	(τ-C5C6)(29) + (ω-C51C52)(11) – (ω-C5C6)(10) – (τ-C60C56)(9) – (ω-C2C9)(9) + (τ-H25O53)(6)
57	402	387	11.45		(ω-C51C52)(28) – (ω-C2C9)(23) – (ω-C5C6)(12) + (τ-H25O53)(8) – (ω-C56C60)(5)

Proposed assignment and potential energy distribution (PED) for vibrational modes: Types of vibrations: ν – stretching, δ_{sc} – scissoring, ρ – rocking, ω – wagging, δ – deformation, δ_{as} – asymmetric deformation, τ – torsion. R – pyrrole ring, R1 – benzene ring.

at higher wavenumber 3465 cm^{-1}, recorded in solution phase [48]. Therefore, solid state spectrum of (**3**) attributes to the vibration of hydrogen bonded N—H group. In dimer, the stretching wavenumber of hydrogen bond donor (N—H) is red-shifted due to its conventional nature with respect to the hydrogen bond free monomer. The observed N—H wagging mode of pyrrole at 774 cm^{-1} correlates with the calculated wavenumber at 790 cm^{-1} in theoretical IR-spectrum. The N—H stretch of acid hydrazide part of molecule is observed at 3391 cm^{-1}, whereas it is calculated at same wave number 3373 cm^{-1} in both monomer and dimer.

Three methyl groups are present in the molecule. They are abbreviated as Me, Me1 and Me2. Me1 and Me2 are directly attached to the C5 and C3 carbon of pyrrole ring. Me is attached to the CH_2 of ester group. In dimer, $\nu_{C—H}$ of Me1 is calculated at higher wavenumber 2937 cm^{-1} (mode no. 215, intensity = 18.34) than the monomer 2930 cm^{-1} (mode no. 104, intensity 17.99). The cause of blue shift in the stretching vibration of hydrogen bond acceptor (C—H) is due to its non-conventional nature than the free C—H vibration in monomer. According to Internal coordinate system recommended by Pulay et al. [36], CH_2 group associate six stretching and bending vibrational frequencies namely: symmetric stretch, asymmetric stretch, scissoring, rocking, wagging and twisting. The scissoring and rocking deformations belong to polarized in-plane vibration whereas wagging and twisting deformations belong to depolarized out-of-plane vibration. The symmetric CH_2 stretching vibrational band observed at 2928 cm^{-1} is in an excellent agreement with the calculated wavenumber at 2944 cm^{-1}. The asymmetric CH_2 stretching vibrational band is assigned at 2984 cm^{-1} but does not observed in experimental FT-IR spectrum. The observed C—H stretching vibrations of benzene ring, ester methyl and ester CH_2 at 3110, 2976 and 2928 cm^{-1} are in agreement with the calculated wavenumber at 3081, 3016 and 2944 cm^{-1} respectively. The observed C—H stretching vibration of hydrazone linkage CH=N at 2863 cm^{-1} correlates with the calculated wavenumber at 2904 cm^{-1} in theoretical IR-spectrum. The observed rocking mode of methyl group at 1058, 1032 cm^{-1} corresponds to the calculated wavenumber at 1086, 1052 cm^{-1} respectively. Asymmetric deformation of pyrrole Me1 group observed at 1500, 1433 cm^{-1} agrees well with the calculated wavenumber at 1508, 1433 cm^{-1} respectively.

The C—C stretches and C—C—H deformations of benzene ring are assigned at 1571, 1159 cm^{-1} respectively. The observed wagging mode of C5—C6 at 655, 695 cm^{-1} correlates with the calculated wavenumber at 667, 692 cm^{-1} respectively. The observed wagging mode of C2—C9 at 439, 511 cm^{-1} agrees well with the calculated wavenumber at 440, 512 cm^{-1} respectively.

The stretching mode of ester carbonyl group ($\nu_{C=O}$) is observed at 1669 cm^{-1}, whereas it is calculated at 1656, 1689 cm^{-1} in dimer and monomer respectively. This shows that observed wavenumber at 1669 cm^{-1} is in good agreement with the calculated wavenumber of dimer. The observed $\nu_{C=O}$ also agrees well with the earlier reported wavenumber at 1665 cm^{-1} for dimer of *syn*-pyrrole-2-carboxylic acid [48]. Therefore, $\nu_{C=O}$ stretching mode in (**3**) confirms the involvement of C=O group in intermolecular hydrogen bonding. The reason for red shift in the stretching wavenumber of hydrogen bond acceptor (C=O) group is due to its involvement in dimer formation by hydrogen bond than free monomer. A combination band of N—H and C=O stretching of acid hydrazide part of molecule is calculated at 1712 cm^{-1} with 27% contribution in PED. The observed C7=N10 stretching vibration ($\nu_{C=N}$) at 1619 cm^{-1} is calculated at same wavenumber in theoretical IR spectrum. The presence of $\nu_{C=N}$ confirms the hydrazone linkage in the product molecule (**3**). The obseved $\nu_{C=N}$ at 1619 cm^{-1} also agrees well with the reported absorption band at 1600 cm^{-1} [49].

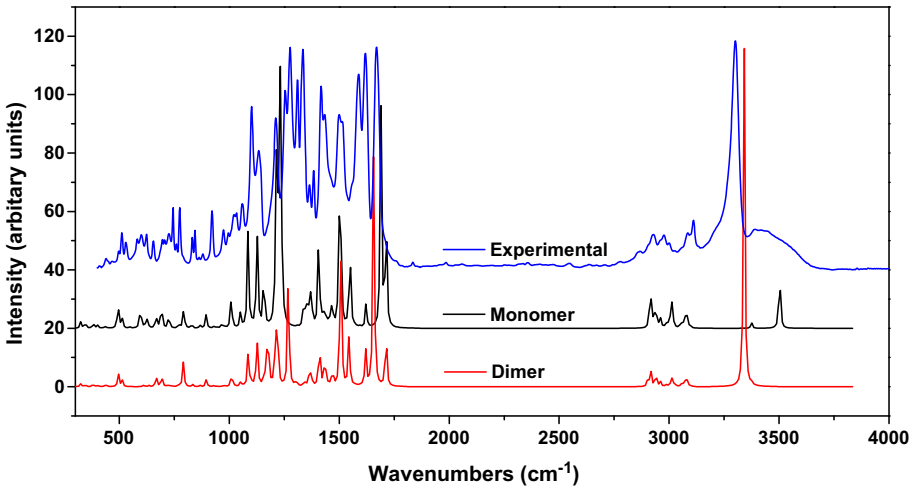

Fig. 7. Correlation graph between experimental and theoretical wavenumbers.

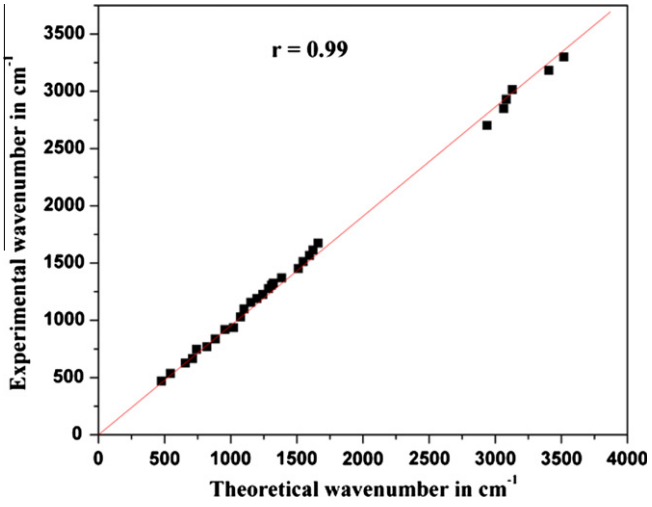

Fig. 8. Correlation graph between experimental and calculated FT-IR wavwnumbers.

4.6. Aim calculation

Geometrical as well as topological parameters are useful tool to characterize the strength of hydrogen bond. The geometrical criteria for the existence of hydrogen bond are as follows: (i) The distance between proton (H) and acceptor (A) to be less than the sum of their van der Waal's radii of these atoms (ii) The 'donor (D)–proton (H)···acceptor (A)' angle to be greater than 90° (iii) The elongation of 'donor (D)-proton(H)' bond length to be observed. These criteria are frequently considered as insufficient, therefore, the existence of hydrogen bond could be supported further by Koch and Popelier criteria [50] based on 'Atoms in Molecules' theory (i) The existence of bond critical point for the 'proton (H)···acceptor (A)' contact (ii) The value of electron density ($\rho_{H\cdots A}$) should be within the range 0.002–0.040 a.u. (iii) The corresponding Laplacian ($\nabla^2\rho_{BCP}$) should be within the range 0.024–0.139 a.u. According to Rozas et al. [51] the H-bonding may be classified as (i) Strong H-bonds: having ($\nabla^2\rho_{BCP}$) < 0 and H_{BCP} < 0, covalent in nature (ii) Medium H-bonds: having ($\nabla^2\rho_{BCP}$) > 0 and H_{BCP} < 0, partially covalent in nature (iii) Weak H-bonds: having ($\nabla^2\rho_{BCP}$) > 0 and H_{BCP} > 0, mainly electrostatic in nature and the distance between interacting atoms is greater than the sum of van der Waal's radii of these atoms.

Molecular graph of the dimer using AIM program at B3LYP/6-31G(d,p) level is shown in Fig. 9. Geometrical parameter – bond length (Å), topological parameters-electron density (ρ_{BCP}), Laplacian of electron density ($\nabla^2\rho_{BCP}$); energetic parameters – kinetic electron energy density (G_{BCP}), potential electron energy density (V_{BCP}), total electron energy density (H_{BCP}), and estimated interaction energy (E_{int}) at bond critical point (BCP) for bonds of interacting atoms in dimer are given in Table 7. The tabulated parameters clearly indicates that there are three types of interactions exist in the dimer (i) O20···H57 are O53···H24 are classical (conventional) moderate hydrogen bonds (ii) O21···H31, O48···H64, O20···H65, O53···H25 are non-conventional (improper) weak hydrogen bonds and (iii) N10···C6, N68···C60 are weak (van der Waal) interactions. Espinosa proposed proportionality between hydrogen bond energy (E) and potential energy density (V_{BCP}) at H···O contact: $E = ½ (V_{BCP})$ [52]. The intermolecular interaction energy of dimer formation as per DFT calculation found to be 14.19 kcal/mol and after BSSE correction 10.63 kcal/mol, whereas per AIM calculations it is 15.19 kcal/mol.

The ellipticity (ε) at BCP is a sensitive index to monitor the π-character of bond. The ε is related to λ_1 and λ_2, which correspond to the eigen values of Hessian and defined as by a relationship: $\varepsilon = (\lambda_1/\lambda_2) - 1$. In order to investigate the effect of π-electron delocalization in bonds associated with N and O atoms of N—H···O heteronuclear intermolecular hydrogen bonds, the analysis of the bond ellipticity is performed. In dimer, intermolecular hydrogen bonds are associated with the 16 member pseudo ring (C9—C2—C3—C4—C5—N1—H19···O60—C52—C48—C46—C44—C47—N50—H56···O14) and abbreviated as R_P. The ε values for bonds involved in pseudo ring (R_P) are given in Table 8. In R_P, the values of ε for bonds O20—C9, C9—C2, C2—C3, C3—C4, C4—C5, C5—N1 associated with the N1—H24···O53 and for bonds O53—C51, C51—C52, C52—C55, C55—C58, C58—C56, C56—N54 associated with the N54—H57···O20 are in the range 0.1015–0.2890. These values of ε correspond to the aromatic bonds reported in literature [53]. The ε values confirm the presence of resonance assisted heteronuclear intermolecular hydrogen bonds because both N and O atoms are interconnected by a system of π-conjugated double bonds.

4.7. Chemical reactivity

4.7.1. Global reactivity descriptors

On the basis of Koopman's theorem, global reactivity descriptors electronegativity (χ), chemical potential (μ), global hardness

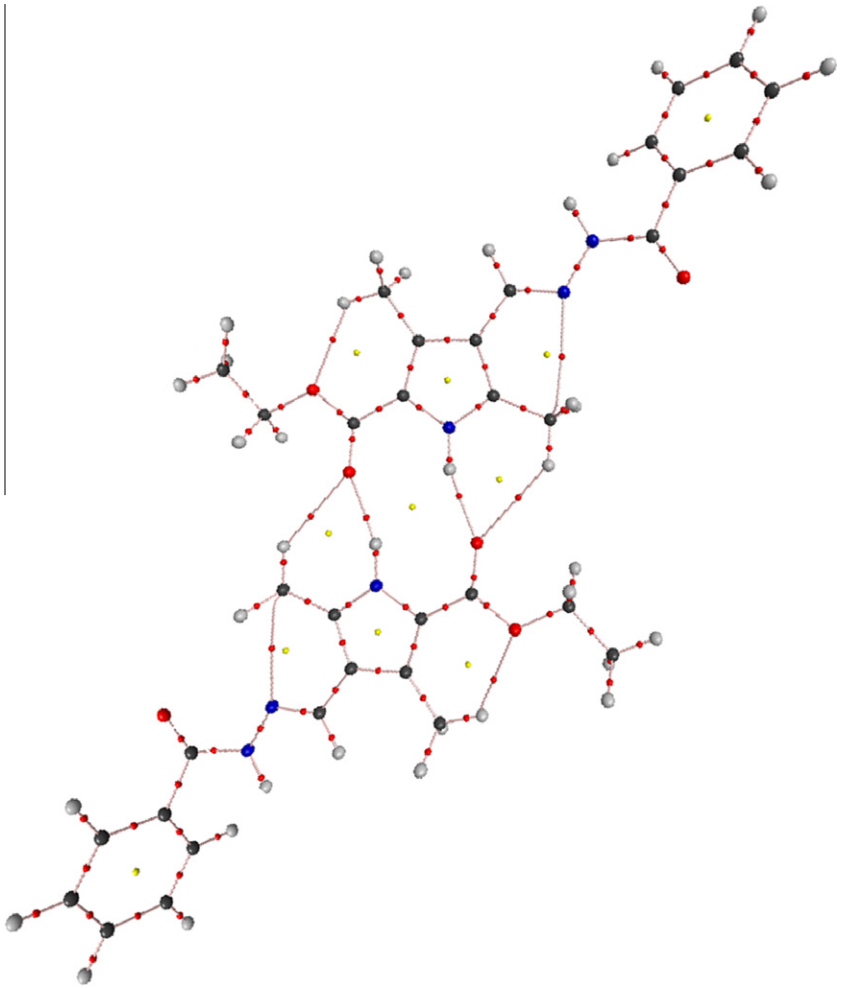

Fig. 9. Molecular graph of dimer: bond critical points (small red spheres), ring critical points (small yellow sphere), bond paths (pink lines) using AIM program. (For interpretation of the references to colour in this figure legend, the reader is referred to the web version of this article.)

Table 7
Geometrical parameter bond length (Å) and topological parameters for bonds of interacting atoms: electron density (ρ_{BCP}), Laplacian of electron density ($\nabla^2\rho_{BCP}$), kinetic electron energy density (G_{BCP}), potential electron energy density (V_{BCP}), total electron energy density (H_{BCP}), estimated interaction energy (E_{int}) at bond critical point (BCP).

Atoms involved in interactions	Bond distance (Å)	ρ_{BCP} (a.u.)	$\nabla^2\rho$(BCP) (a.u.)	G_{BCP} (a.u.)	V_{BCP} (a.u.)	H_{BCP} (a.u.)	Bond degree	E_{int} (kcal/mol)
O20···H57	1.9073	0.0254	0.0820	0.0199	−0.0194	0.0005	0.0213	−6.0
O53···H24	1.9074	0.0254	0.0819	0.0199	−0.0194	0.0005	0.0213	−6.0
O21···H31	2.3054	0.0144	0.0484	0.0113	−0.0105	0.0007	0.0544	−3.3
O48···H64	2.3053	0.0144	0.0484	0.0113	−0.0105	0.0007	0.0544	−3.3
N10···C6	3.0351	0.0087	0.0344	0.0070	−0.0055	0.0015	0.1730	−1.7
N68···C60	3.0351	0.0087	0.0344	0.0070	−0.0055	0.0015	0.1730	−1.7
O20···H65	2.5957	0.0074	0.0260	0.0056	−0.0048	0.0008	0.1158	−1.5
O53···H25	2.5958	0.0074	0.0260	0.0056	−0.0048	0.0008	0.1158	−1.5

Table 8
Ellipticity parameters for bonds of sixteen member pseudo ring (R_P).

Bond	ε	Bond	ε
O20—C9	0.1015	O53—C51	0.1015
C9—C2	0.2281	C51—C52	0.2281
C2—C3	0.2890	C52—C55	0.2890
C3—C4	0.2204	C55—C58	0.2204
C4—C5	0.2521	C58—C56	0.2521
C5—N1	0.1690	C56—N54	0.1690
N1···H24	0.0308	N54···H57	0.0308
H24···O53	0.0202	H57···O20	0.0202

(η), global softness (S) and global electrophilicity index (ω) are calculated using the energies of frontier molecular orbitals ε_{HOMO}, ε_{LUMO} and given by Eqs. (1)–(5) [54,55]

$$\chi = 1/2(\varepsilon_{LUMO} + \varepsilon_{HOMO}) \quad (1)$$

$$\mu = \chi = 1/2(\varepsilon_{LUMO} + \varepsilon_{HOMO}) \quad (2)$$

$$\eta = 1/2(\varepsilon_{LUMO} - \varepsilon_{HOMO}) \quad (3)$$

$$S = 1/2\eta \quad (4)$$

$$\omega = \mu^2/2\eta \quad (5)$$

Electrophilicity index (ω) measures the stabilization in energy when the system acquires an additional electronic charge (ΔN_{max})

Table 9
ε_{HOMO}, ε_{LUMO}, energy gap ($\varepsilon_{LUMO} - \varepsilon_{HOMO}$), chemical potential ($\mu$), electronegativity ($\chi$), global hardness ($\eta$), global softness ($S$) and global electrophilicity index (ω).

Molecules	ε_H (eV)	ε_L (eV)	$(\varepsilon_L - \varepsilon_H)$ (eV)	χ (eV)	μ (eV)	η (eV)	S (eV^{-1})	ω (eV)
Reactant (1)	−6.16	−1.01	5.14	3.58	−3.58	2.57	0.19	2.50
Reactant (2)	−6.54	−0.86	5.68	3.70	−3.70	2.84	0.17	2.41
Product (3)	−5.47	−1.21	4.25	3.34	−3.34	2.12	0.23	2.63

Table 10
Electrophilic reactivity descriptors (f_k^+, s_k^+, ω_k^+) of (**1**) and nucleophilic reactivity descriptors (f_k^-, s_k^-, ω_k^-) of (**2**) for selected atomic sites, using Hirshfeld atomic charges.

Reactant (1)	f_k^+, (e)	s_k^+ (eV^{-1})	ω_k^+ (eV)	Reactant (**2**)	f_k^- (e)	s_k^- (eV^{-1})	ω_k^- (eV)
C7	0.1479	0.0287	0.3702	N9	0.0916	0.0161	0.2214
C10	0.0921	0.0179	0.2305	N10	0.1105	0.0194	0.2670

from the environment. The energies of frontier molecular orbitals (ε_{HOMO}, ε_{LUMO}), energy gap ($\varepsilon_{LUMO} - \varepsilon_{HOMO}$), electronegativity ($\chi$), chemical potential ($\mu$), global hardness ($\eta$), global softness ($S$) and global electrophilicity index (ω) for reactants **1**, **2** and product (**3**) are listed in Table 9. The calculated high value of (ω) for (**3**) shows that the title molecule to be a strong electrophile than reactants **1** and **2**.

4.7.2. Local reactivity descriptors

Fukui functions (f_k^+, f_k^-, f_k^0), local softnesses (s_k^+, s_k^-, s_k^0) and local electrophilicity indices (ω_k^+, ω_k^-, ω_k^0) have been described earlier in literature [56,57]. Using Hirshfeld population analyses of neutral, cation and anion state of molecule, Fukui Functions are calculated at same calculation method B3LYP/6-31G(d,p) using following equations:

$$f_k^+ = [q(N+1) - q(N)] \quad \text{for nucleophilic attack} \tag{6}$$

$$f_k = [q(N) - q(N-1)] \quad \text{for electrophilic attack} \tag{7}$$

$$f_k^0 = 1/2[q(N+1) + q(N-1)] \quad \text{for radical attack} \tag{8}$$

where N, N − 1, N + 1 are total electrons present in neutral, cation and anion state of molecule respectively.

Local softnesses and electrophilicity indices are calculated using the following equations:

$$S_k^+ = Sf_k^+, \quad s_k = Sf_k^-, \quad s_k^0 = Sf_k^0 \tag{9}$$

$$\omega_k^+ = \omega f_k^+, \quad \omega_k = \omega f_k^-, \quad \omega_k^0 = \omega f_k^0 \tag{10}$$

where +, −, 0 signs show nucleophilic, electrophilic and radical attack respectively.

Local electrophilic reactivity descriptors (f_k^+, s_k^+, ω_k^+) for selected atomic sites of (**1**) and nucleophilic reactivity descriptors (f_k^-, s_k^-, ω_k^-) for selected atomic sites of (**2**) are listed in Table 10, using Hirshfeld population analyses respectively. The maximum values of (f_k^+, s_k^+, ω_k^+) at C7 in (**1**) indicate that this is most reactive site for nucleophilic attack. The maximum values of (f_k^-, s_k^-, ω_k^-) at C10 in (**2**) indicate that this is most nucleophilic site. Therefore, formation of product (**3**) is confirmed by the attack of C10 site of (**2**) on C7 site in (**1**).

Fukui functions (f_k^+, f_k^-), Local softnesses (s_k^+, s_k^-), Local electrophilicity indices (ω_k^+, ω_k^-) for selected atomic sites of (**3**) are listed in Table 11 using Hirshfeld population analyses. The high values of all the three local electrophilic reactivity descriptors (f_k^+, s_k^+, ω_k^+) at C7 indicate that this site is more prone to nucleophilic attack. The calculated local reactivity descriptors of synthesized molecule (**3**) favor the formation of new heterocyclic compounds such as azetidinones, oxadiazolines and thiazolidinones by attack of nucleophilic part of the dipolar reagent on the C7 site and electrophilic part of dipolar reagent on the N10 site of C7═N10 bond.

Table 11
Electrophilic reactivity descriptors (f_k^+, s_k^+, ω_k^+) and nucleophilic reactivity descriptors (f_k^-, s_k^-, ω_k^-) for selected atomic sites of (**3**), using Hirshfeld atomic charges.

Atom no.	f_k^+ (e)	f_k^- (e)	s_k^+ (eV^{-1})	s_k^- (eV^{-1})	ω_k^+ (eV)	ω_k^- (eV)
N1	0.0259	0.0582	0.0060	0.0136	0.0682	0.1531
C2	0.0239	0.0743	0.0055	0.0171	0.0630	0.1956
C3	0.0366	0.0231	0.0084	0.0053	0.0964	0.0608
C4	0.0045	0.0672	0.0010	0.0154	0.0118	0.1769
C5	0.0184	0.0760	0.0042	0.0175	0.0486	0.2002
C6	0.0352	0.0862	0.0081	0.0198	0.0928	0.2268
C7	0.1011	0.0679	0.0233	0.0156	0.2662	0.1787
C8	0.0377	0.0645	0.0087	0.0148	0.0993	0.1697
C9	0.0332	0.0168	0.0076	0.0038	0.0875	0.0443
N10	0.0534	0.0520	0.0123	0.0119	0.1407	0.1369
N11	0.0303	0.0834	0.0069	0.0192	0.0798	0.2196
C12	0.0595	0.0243	0.0137	0.0056	0.1567	0.0641
O13	0.0863	0.0543	0.0199	0.0125	0.2272	0.1430
C14	0.0291	−0.0020	0.0067	−0.0004	0.0768	−0.0053
C15	0.0505	0.0061	0.0116	0.0014	0.1331	0.0162
C16	0.0569	0.0278	0.0131	0.0064	0.1498	0.0732
C17	0.0965	0.0437	0.0222	0.0100	0.2541	0.1150
C18	0.0608	0.0342	0.0140	0.0079	0.1600	0.0902
C19	0.0550	0.0207	0.0126	0.0047	0.1448	0.0546
O20	0.0473	0.0521	0.0109	0.0120	0.1246	0.1372
O21	0.0133	0.0149	0.0030	0.0034	0.0351	0.0393
C22	0.0218	0.0265	0.0050	0.0061	0.0575	0.0698
C23	0.0214	0.0271	0.0049	0.0062	0.0565	0.0714

5. Conclusions

In the present study, compound (**3**) has been synthesized and characterized by ^{1}H NMR, UV–Vis, FT-IR and mass spectroscopy. Experimental electronic absorption spectra have some blue shifts compared with theoretical data and NBO analysis suggests that electronic transitions are $\pi \rightarrow \pi^*$ and $n \rightarrow \pi^*$ in nature. The experimental vibrational wavenumbers agree well with the calculated wavenumbers of dimer, support the existence of dimer in the solid state. A combined experimental and theoretical vibrational analysis shows that in conventional intermolecular hydrogen bridge (N—H···O═C) the stretching wavenumber of both N—H and C═O are red-shifted due to the bond elongation. In contrary, the stretching wavenumber of C—H in non-conventional intermolecular hydrogen bridge (C—H···O═C) is blue-shifted due to the bond contraction. The energy of each heteronuclear intermolecular hydrogen bond (N—H···O) is calculated as −6.0916 kcal/mol. AIM ellipticity analysis confirms the presence of resonance assisted intermolecular hydrogen bonds in dimer. In addition, theoretical results from reactivity descriptors are in complete agreement with observed reactivity of such type of compounds. The local electronic reactivity descriptors show that azomethine carbon (C7) is more reactive site for nucleophilic attack and may be used as precursor for the syntheses of new heterocyclic compounds such as azetidinones, oxadiazolines and thiazolidinones.

Acknowledgments

The authors are thankful to the DST New Delhi for financial supports.

References

[1] M. Yu, H. Lin, Ind. J. Chem. Sec. A 46 (2007) 1437.
[2] A. Rauf, M.R. Banday, R.H. Mattoo, Acta Chim. Slov. 55 (2008) 448.
[3] S. Rollas, N. Gülerman, H. Erdeniz, Farmaco 57 (2002) 171.
[4] V.O. Kozminykh, A.O. Belyaev, Bukanova, E.V. Kozminykh, T.F. Odegova, J. Pharm. Chem. 38 (2004) 368.
[5] L.W. Zheng, L.L. Wu, B.X. Zhao, W.L. Dong, J.Y. Miao, Bioorg. Med. Chem. 17 (2009) 1957.
[6] D. Sriram, P. Yogeeswari, R.V. Devakaram, Bioorg. Med. Chem. 14 (2006) 3113.
[7] T.L. Smalley, A.J. Peat Jr., J.A. Boucheron, S. Dickerson, D. Garrido, F. Preugschat, S.L. Schweiker, S.A. Thomson, T.Y. Wang, Bioorg. Med. Chem. 16 (2006) 2091.
[8] N. Raman, S. Ravichandran, C. Thangaraja, J. Chem. Sci. 116 (2004) 215.
[9] J.P. Jasinski, C.J. Guild, C.S.C. Kumar, H.S. Yathirajan, A.N. Mayekar, Bull. Korean Chem. Soc. 31 (2010) 881.
[10] L. Lalib, L.A. Mohamed, M.F. Iskander, Transition Met. Chem. 25 (2002) 700.
[11] M.A. Affan, I.P.P. Foo, B.A. Fasihuddin, E.U.H. Sim, M.A. Hapipah, J. Anal. Sci. 13 (2009) 73.
[12] M. Yu, H. Lin, H. Lin, Ind. J. Chem. Sec. A 46 (2007) 1437.
[13] B. Szczesna, U. Lipkowska, Supramol. Chem. 13 (2001) 247.
[14] S. Vijayakumar, A. Adithya, K.N. Sharafudeen, B.K. Chandrasekharan, J. Mod. Optic 57 (2010) 670.
[15] X. Deng, N.S. Mani, Org. Lett. 10 (2008) 1307.
[16] X. Deng, N.S. Mani, J. Org. Chem. 73 (2008) 2412.
[17] Y. Nakayama, Y. Sanemitsu, J. Org. Chem. 49 (1984) 1703.
[18] H.N. Dogan, A. Duran, S. Rollas, G. Sener, Y. Armutak, M.K. Uysal, Med. Sci. Res. 26 (1998) 755.
[19] S.G. Küçükgüzel, A. Kocatepe, E. De Clercq, F. Sahin, Eur. J. Med. Chem. 41 (2006) 353.
[20] S.G. Küçükgüzel, E.E. Oruç, S. Rollas, F. Sahin, A. Ozbek, Eur. J. Med. Chem. 37 (2002) 197.
[21] V.N. Korotchenko, A.V. Shastin, V.G. Nenaidenko, E.S. Balenkova, Russ. J. Org. Chem. 39 (2003) 527.
[22] L.E. Kaïm, L. Gautier, L. Grimaud, L.M. Harwood, V. Michaut, Green Chem. 54 (2003) 779.
[23] A. Kotali, I.S. Lafazanis, Arkivoc vi (2003) 91.
[24] S. Scheiner, Y. Gu, T. Kar, J. Mol. Struct.: Theochem 500 (2000) 441.
[25] F.H. Allen, V.J. Hoy, J.A.K. Howard, V.R. Thalladi, G.R. Desiraju, C.C. Wilson, G. McIntyre, J. Am. Chem. Soc. 119 (1997) 3477.
[26] D. Philp, J.M.A. Robinson, J. Chem. Soc. Perkin Trans. 2 (1998) 1643.
[27] E.J.H. Chu, T.C. Chu, J. Org. Chem. 19 (1954) 266.
[28] Frisch et al., Gaussian 09 2004 Revision C.02, Gaussian, Inc., Wallingford, CT.
[29] A.D. Becke, J. Chem. Phys. 98 (1993) 5648.
[30] C.T. Lee, W.T. Yang, R.G.B. Parr, Phys. Rev. 37 (1988) 785.
[31] D.A. Petersson, M.A. Allaham, J. Chem. Phys. 94 (1991) 6081.
[32] G.A. Petersson, A. Bennett, T.G. Tensfeldt, M.A. Allaham, W.A.J. Mantzaris, J. Chem. Phys. 89 (1988) 2193.
[33] G.A. Zhurko, D.A. Zhurko, Chemcraft, lite version build 08 (freeware), 2005.
[34] Computer program Gauss-view 3.09, Ver 2, Gaussian Inc, Pittsburgh, PA.
[35] J.M.L. Martin, V. Alsenoy, C.V. Alsenoy, Gar2ped, University of Antwerp, 1995.
[36] P. Pulay, G. Fogarasi, F. Pang, J.E. Boggs, J. Am. Chem. Soc. 101 (1979) 2550.
[37] R.F.W. Bader, Atoms in Molecules, A Quantum Theory, Oxford University Press, Oxford, 1990.
[38] J. Miroslaw, P. Marcin, J. Phys. Chem. A 114 (2010) 2240.
[39] S.F. Boys, F. Bernardi, Mol. Phys. 19 (1970) 553.
[40] Dao-Xin Wu, Tian Lin, Jiong Sun, Ming-Zhi Huang, Z. Kristallogr. NCS 224 (2009) 229–230.
[41] C.T. Arrannja, M.R. Siva, A.M. Beja, A.F. Ferreira, A.J. Sobral, Acta Cryst. E64 (2008) o1989.
[42] M.G. Gardiner, R.C. Jones, S. Smith, Acta Cryst. E63 (2007) o470.
[43] M.O. Senge, K.M. Smith, Acta Cryst. C61 (2005) o537.
[44] M.C. Etter, Acc. Chem. Res. 23 (1990) 120.
[45] K. Wolinski, J.F. Hinton, J.F. Pulay, J. Am. Chem. Soc. 112 (1990) 8251.
[46] D. Jackuemin, E.A. Perpète, J. Mol. Struct. Theochem 804 (2007) 31.
[47] N. Sundaraganesan, E. Kavitha, S. Sebastian, J.P. Cornard, M. Martel, Spectrochim. Acta Part A Mol. Biomol. Spectrosc. 74 (2009) 88.
[48] A.T. Dubis, S.J. Grabowski, D.B. Romanowska, T. Misiaszek, J. Leszczynski, J. Phys. Chem. A 106 (2002) 10613.
[49] J. El Mostapha, A. Riou, M. Allain, M.A. Khan, G. Bouet, Polyhedron 20 (2001) 67.
[50] U. Koch, P. Popelier, J. Phys. Chem. A 99 (1995) 9747.
[51] I. Rozas, I. Alkorta, J. Elguero, J. Am. Chem. Soc. 122 (2000) 11154.
[52] E. Espinosa, E. Molins, C. Lecomte, Chem. Phys. Lett. 285 (1998) 170.
[53] C.F. Matta, R.J. Boyd, The Quantum Theory of Atoms in Molecules, Wiley-VCH, Verlag-Gmbh, 2007, p. 12 (Chapter 1).
[54] R.G. Parr, R.G. Pearson, J. Am. Chem. Soc. 105 (1983) 7512.
[55] P. Geerlings, F. De Proft, W. Langenaeker, Chem. Rev. 103 (2003) 1793.
[56] L. Szentpály, S. Liu, J. Am. Chem. Soc. 121 (1999) 1922.
[57] P.K. Chattaraj, S. Giri, J. Phys. Chem. A 111 (2007) 11116.